ISA Journal of Engineering and Technology (ISAJET)

Homepage: https://isapublisher.com/isajet/

Volume 3, Issue 5, Sept-Oct, 2026 ISSN: 3049-1843

Land-Cover Change, Runoff Propensity, Road Drainage and Pavement Condition in Aba, Nigeria: A Scale-Aware Assessment

Obianyo, J.I. & Ugorji S.A.

Department of Civil Engineering, Michael Okpara University of Agriculture, Umudike, Umuahia, Abia State, Nigeria

Received: *10.08.2026* | ***Accepted:*** *01.09.2026* | ***Published:*** *20.09.2026*

***Corresponding Author:** Obianyo, J.I.

DOI: *10.5281/zenodo.22856173*

Abstract **Original Research Article**

Urban expansion and inadequate drainage influence pavement performance across different spatial scales. This study assessed land-cover change, runoff propensity, drainage condition and pavement condition in Aba, Nigeria, using two related but analytically separate pathways. Dynamic World V1 land-cover maps for 2015, 2020 and 2025 were classified into built-up area, vegetation, bare land and water. The proportional area of each class was combined with fixed screening coefficients derived from HEC-22 to determine a dimensionless weighted runoff-propensity coefficient (Cw). Drainage and pavement-condition data from thirteen purposively selected road corridors were analysed using a study-specific Drainage Condition Index (DCI) and a length-based Pavement Condition Index (PCI-L). Between 2015 and 2025, built-up area increased from 477.24 to 634.79 km², while vegetation decreased from 241.88 to 90.85 km². Over the same period, Cw increased from 0.710650 to 0.854725, indicating greater relative surface-runoff propensity. The fitted corridor model, PCI-L = -7.0564 + 1.0801(DCI), accounted for 42.9 per cent of the observed variation in pavement condition. The association was significant under conventional ordinary least squares estimation ($p = 0.0151$), while HC3 covariance estimation yielded $p = 0.0553$, showing that the strength of the statistical evidence varied with the uncertainty estimator. East Road, Okigwe Road, Ezi-Ukwu Road and Mosque Road were classified as high-priority corridors. The results support land-cover monitoring, drainage inspection and targeted pavement assessment while maintaining a clear distinction between planning-level screening and hydraulic or structural design.

Keywords: land-cover; runoff propensity; road drainage; pavement condition; scale-aware assessment.

1. Introduction

Pavement condition reflects traffic loading, structural capacity, materials, environmental exposure, construction quality and maintenance. In humid tropical settings, poor drainage and prolonged moisture exposure reduce the stiffness and bearing resistance of unbound layers and subgrade, accelerating rutting, cracking, pumping, stripping and material loss. Drainage is therefore an important pavement-system component, but deterioration also depends on pavement age, layer thickness, material quality, traffic and maintenance history (Chu et al., 2023; Mousavi et al., 2021; Silva et al., 2021).

Urban expansion adds hydrological pressure by replacing permeable surfaces with buildings and roads, reducing interception and infiltration and concentrating runoff in drains and receiving channels. Runoff response depends on impervious-cover connectivity, terrain, rainfall and drainage continuity (Idowu & Zhou, 2021; Zhang et al., 2022). Satellite products support consistent monitoring where ground observations are limited. Dynamic World provides 10 m Sentinel-2-based land-cover information, while CHIRPS combines satellite rainfall estimates with station observations at 0.05° resolution (Brown et al., 2022).

Flooding in West African cities reflects interacting deficiencies in spatial planning, drainage provision, environmental management, maintenance, governance and rainfall response (Abeka et al., 2020). Nigerian evidence also links inadequate open drainage and expanding impervious surfaces with infrastructure damage (Fayomi et al., 2024). Aba is densely developed, has low relief and persistent drainage constraints, while an earlier GIS assessment identified elevation, slope and rainfall as components of local flood vulnerability (Ogbonna et al., 2015).

Land-cover and hydrological studies commonly operate at catchment or city scale, whereas pavement-condition studies rely on road-section observations (Piryonesi and El-Diraby, 2020; Zhang et al., 2022). This study therefore keeps the three city-scale land-cover benchmarks separate from the thirteen road corridors and integrates them only for engineering interpretation and maintenance prioritisation. The objectives were to quantify land-cover change, determine a comparative weighted runoff-propensity coefficient, describe corridor drainage and pavement condition, test the DCI-PCI-L association with robustness diagnostics, and integrate the two analytical pathways without statistical pooling.

2. Materials and methods

2.1 Study area and scale-aware research design

The analysis covered the 766.65 km² Aba urban boundary in Abia State, southeastern Nigeria, approximately 5°04′-5°10′ N and 7°19′-7°23′ E, associated with Aba North, Aba South, Osisioma Ngwa, Obingwa and Ugwunagbo Local Government Areas. The humid tropical climate, low relief and dense development influence runoff routing, drainage performance and pavement moisture exposure. The city-scale pathway assessed 2015, 2020 and 2025 land cover and runoff propensity, while the corridor pathway assessed drainage and pavement condition on thirteen selected roads. The datasets were analysed separately because they represent different spatial units and were combined only for engineering decision support.

Table 1. Data sources, analytical scales, outputs and analytical scope

Component and objective	Data and analytical unit	Observations	Output	Analytical scope
Land-cover change	Dynamic World V1 land-cover maps within the 766.65 km² analytical boundary	2015, 2020 and 2025	Four harmonised classes and benchmark changes	Comparative land-cover assessment across the three benchmark years

Rainfall context	CHIRPS v2.0 monthly rainfall values from the USGS FEWS Early Warning Explorer	36 monthly values	Climatic context and rainfall summary	Climatic characterisation; excluded from runoff and hydraulic calculations
Runoff propensity	Benchmark class areas and fixed HEC-22-based screening coefficients	Three benchmark years	Dimensionless weighted runoff-propensity coefficient, Cw	Relative comparison of land-cover-based runoff propensity
Road-corridor screening	Pavement failure lengths and nominal dual-side drainage lengths	13 road corridors	DCI, PCI-L and maintenance-priority class	Study-specific screening of purposively selected corridors
Scale-specific modelling	DCI and PCI-L	n = 13	Linear association model and robustness diagnostics	In-sample association evaluated with robust and leave-one-out diagnostics

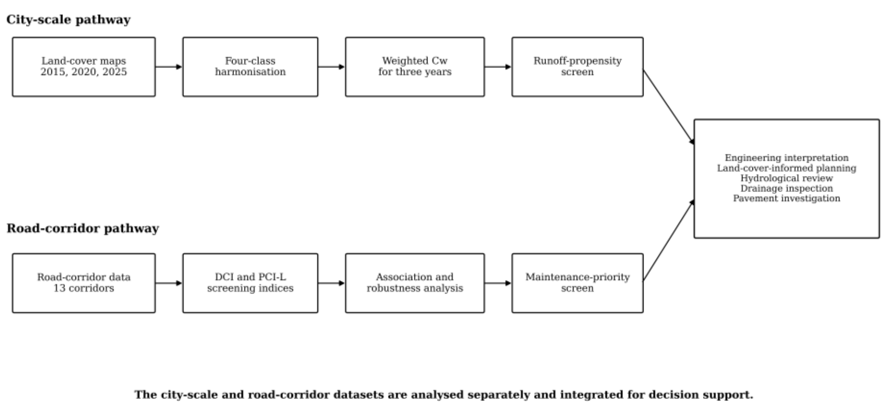

Figure 1. Scale-aware analytical framework linking the city-scale land-cover and runoff-propensity pathway with the road-corridor drainage and pavement pathway. The two datasets were analysed separately and integrated during engineering interpretation.

2.2 Land-cover and rainfall data

Land-cover analysis used the Google Earth Engine Dynamic World V1 dataset (GOOGLE/DYNAMICWORLD/V1), which provides Sentinel-2-based labels and nine class-probability bands at 10 m resolution (Brown et al., 2022; Google Earth Engine, n.d.-b). ArcMap 10.7.1 was used for clipping, overlay, area calculation and map preparation. The built class represented built-up area; trees, grass, flooded vegetation, crops and shrub or scrub were grouped as vegetation; bare ground and water remained separate. Annual totals were checked against 766.65 km². Dynamic World coverage began on 27 June 2015, so the 2015 benchmark represents the available part of that year. Interpretation followed established principles of classification accuracy and area estimation (Olofsson et al., 2014; Venter et al., 2022).

Monthly rainfall for 2015, 2020 and 2025 was obtained from CHIRPS v2.0 through the USGS FEWS Early Warning Explorer. CHIRPS combines satellite rainfall estimates with ground observations at 0.05° resolution (Funk et al., 2015; Google Earth Engine, n.d.-a). Twelve monthly values were analysed per benchmark year, giving mean monthly rainfall of 175.00 mm in 2015, 179.16 mm in 2020 and 197.30 mm in 2025. Rainfall characterised the benchmark climate and was not used in the runoff-propensity coefficient. Land-cover change was calculated as absolute change, percentage change and average annual change.

$Absolute\ change = A_2 - A_1$	(1)
$\Delta A\ (\%) = [(A_2 - A_1) / A_1] \times 100$	(2)
$Annual\ rate = (A_2 - A_1) / (t_2 - t_1)$	(3)

2.3 Weighted runoff-propensity analysis

For each benchmark year, the proportional area of the four land-cover classes was combined with fixed screening coefficients of 0.95 for built-up area, 0.25 for vegetation, 0.40 for bare land, and 1.00 for water. The values were selected from HEC-22 Rational Method coefficient ranges (Federal Highway Administration [FHWA], 2024). Cw is a dimensionless comparative indicator of land-cover-related runoff propensity. It is not runoff depth, volume, peak discharge or drainage capacity, which require locally calibrated hydrological and hydraulic inputs.

$$Cw = \Sigma(A_i C_i) / \Sigma A_i \quad (4)$$

2.4 Road-corridor condition and screening indices

The corridor assessment covered Aba Owerri Road, Faulks Road, Ogbor Hill Road, East Road, Ngwa Road, Azikiwe Road, Okigwe Road, Osusu Road, Omuma Road, Ezi-Ukwu Road, Ehi Road, Mosque Road and Port Harcourt Road. Selection was purposive. Pavement records contained total corridor length, failed pavement length and observed distress types. Drainage screening used a nominal dual-side reference length equal to twice road length, with failure identified from blockage, siltation, ponding, outlet defects, shoulder erosion, collapsed sections, cracking and obstruction. Surveyed route limits, measured lengths, distress descriptions and photographs supported the corridor assessment.

DCI expresses the proportion of the nominal dual-side drainage length not classified as failed, while PCI-L expresses the proportion of surveyed pavement length not classified as failed. PCI-L is a study-specific length-based measure and does not replace the ASTM D6433 Pavement Condition Index, which uses distress type, severity, density, deduct values and corrected deduct values (ASTM, 2024). Index values of 90-100 were classed as excellent, 80-89.99 good, 70-79.99 fair, 60-69.99 poor and below 60 very poor. High maintenance priority was assigned where either index was below 80 per cent, low priority where both were at least 90 per cent, and medium priority otherwise.

$$DCI\ (\%) = [1 - (Ldf / Ldt)] \times 100 \quad (5)$$

$$PCI - L\ (\%) = [1 - (Lpf / Lpt)] \times 100 \quad (6)$$

2.5 Statistical analysis and software

Ordinary least squares assessed the association between DCI and PCI-L across the thirteen corridors, with DCI as explanatory variable and PCI-L as response. The relationship was treated as an in-sample association. Land-cover and Cw changes were evaluated descriptively across the three benchmark years. Model evaluation included coefficient estimates, confidence intervals, R^2, adjusted R^2, MAE, RMSE, MAPE, mean bias, Pearson and Spearman correlations, and residual tests. MAE and RMSE were reported together because they characterise error magnitude differently (Willmott and Matsuura, 2005).

The conventional OLS slope was supplemented by HC3 covariance estimates, a 20,000-replicate pairs bootstrap and leave-one-out refitting. Externally studentised residuals, leverage, Cook's distance and DFFITS identified influential observations (Belsley et al., 1980; Cook, 1977). Analyses and publication figures were prepared in Python 3.13.5 using pandas 2.2.3, NumPy 2.3.5, SciPy 1.17.0, statsmodels 0.14.6 and Matplotlib 3.10.8; ArcMap 10.7.1 supported spatial processing and map preparation.

$$PCI - L = \beta_0 + \beta_1 DCI + \varepsilon \quad (7)$$

3. Results

3.1 Land-cover and runoff-propensity results

The analytical area totalled 766.65 km² in each benchmark. Built-up cover increased from 477.24 km² (62.25 per cent) in 2015 to 571.92 km² (74.60 per cent) in 2020 and 634.79 km² (82.80 per cent) in 2025. Vegetation declined from 241.88 to 150.26 and 90.85 km², bare land from 27.60 to 23.77 and 19.17 km², while water increased from 19.93 to 20.70 and 21.85 km². Over 2015-2025, built-up area gained 157.55 km² and vegetation lost 151.03 km²; average annual built-up increase slowed from 18.94 km² per year in 2015-2020 to 12.57 km² per year in 2020-2025.

Table 2. Land-cover areas and weighted runoff-propensity results for the benchmark years

Indicator	2015	2020	2025	2015-2025 change
Built-up area, km²	477.24	571.92	634.79	+157.55, +33.01%
Vegetation, km²	241.88	150.26	90.85	-151.03, -62.44%
Bare land, km²	27.60	23.77	19.17	-8.43, -30.56%
Water, km²	19.93	20.70	21.85	+1.92, +9.62%
Weighted runoff-propensity coefficient, Cw	0.710650	0.797100	0.854725	+0.144075, +20.27%

Note: Cw is a dimensionless comparative indicator calculated with fixed coefficients derived from HEC-22 Rational Method ranges. Values were calculated from full-precision class areas, while displayed areas are rounded.

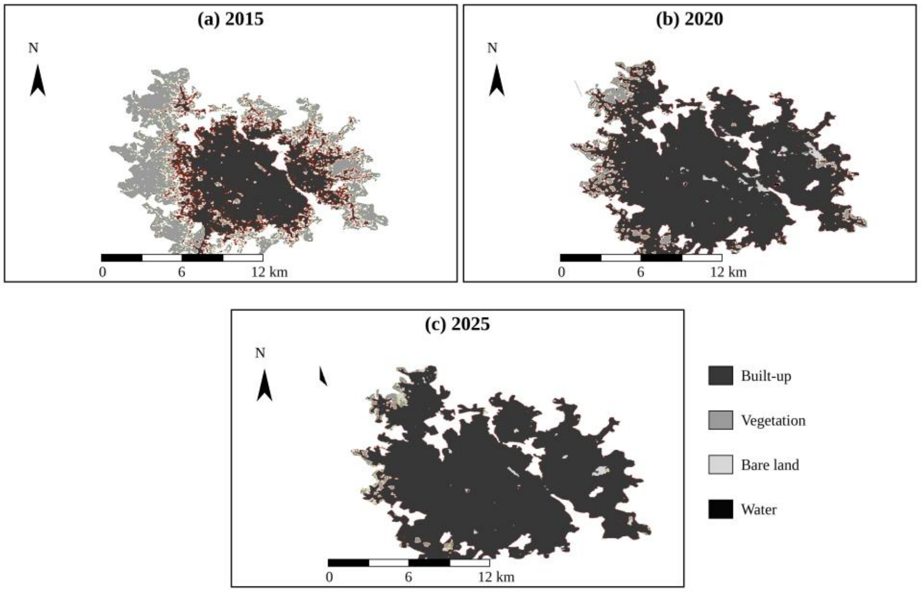

Figure 2. Harmonised Dynamic World V1 land-cover benchmark maps for (a) 2015, (b) 2020 and (c) 2025, arranged in a common layout for comparison across the study period.

Cw increased from 0.710650 in 2015 to 0.797100 in 2020 and 0.854725 in 2025. The increase was 12.16 per cent in 2015-2020, 7.23 per cent in 2020-2025 and 20.27 per cent over the full period. Because the screening constants were fixed, the change reflects mapped land-cover composition, principally built-up expansion and vegetation loss. The 2025 configuration therefore had greater relative propensity for rapid surface-runoff generation than the 2015 configuration.

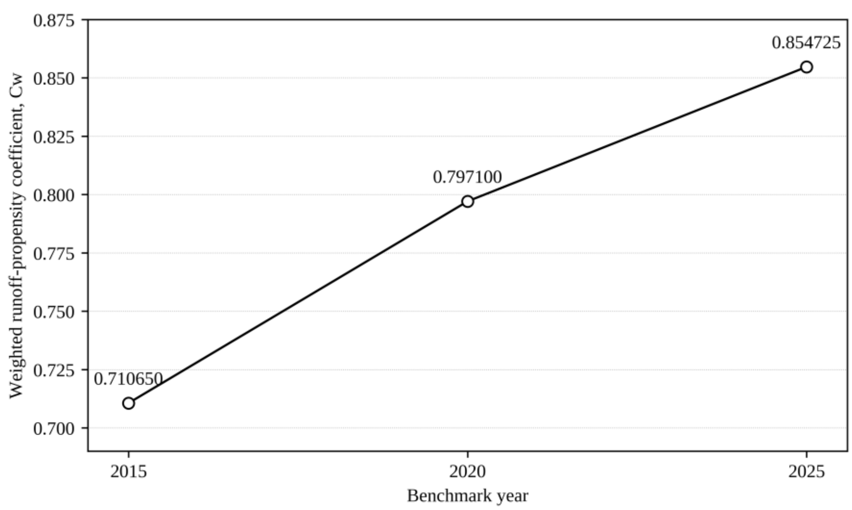

Figure 3. Weighted runoff-propensity coefficient for the three mapped benchmark years.

3.2 Road-corridor condition and model diagnostics

DCI ranged from 79.34 to 92.00 per cent and PCI-L from 70.90 to 97.43 per cent. Port Harcourt Road recorded the highest values for both indices, while East Road had the lowest DCI and Mosque Road the lowest PCI-L. East Road, Okigwe Road, Ezi-Ukwu Road and Mosque Road were high priority; Aba Owerri Road, Ogbor Hill Road and Port Harcourt Road were low priority; the remaining corridors were medium priority.

Table 3. Drainage condition, pavement condition and maintenance-priority classification of the surveyed corridors

Road corridor	DCI, %	PCI-L, %	Priority
Aba Owerri Road	91.49	92.40	Low
Faulks Road	90.91	87.79	Medium
Ogbor Hill Road	91.39	94.07	Low
East Road	79.34	90.98	High
Ngwa Road	84.22	85.24	Medium
Azikiwe Road	87.63	87.44	Medium
Okigwe Road	80.52	78.83	High
Osusu Road	82.77	83.72	Medium
Omuma Road	82.99	84.27	Medium
Ezi-Ukwu Road	81.60	75.54	High
Ehi Road	86.39	83.26	Medium
Mosque Road	83.08	70.90	High
Port Harcourt Road	92.00	97.43	Low

Note: DCI uses a nominal dual-side corridor length defined as twice road length. PCI-L is a study-specific length-based index and differs from the deduct-value Pavement Condition Index defined by ASTM D6433.

The fitted equation was PCI-L = -7.0564 + 1.0801(DCI). The OLS slope was 1.0801 (SE = 0.3757, $t = 2.8747$, $p = 0.0151$, 95 per cent CI 0.2531-1.9071), with $R^2 = 0.4290$, adjusted $R^2 = 0.3771$ and $F(1,11) = 8.264$. MAE was 3.83, RMSE 5.42, MAPE 4.63 per cent and mean bias approximately zero. Pearson r was 0.655 ($p = 0.0151$) and Spearman rho 0.643 ($p = 0.0178$). HC3 covariance increased the slope SE to 0.5039 and gave $p = 0.0553$ (95 per cent interval -0.0289 to 2.1891), while the 20,000-

replicate bootstrap gave a median slope of 1.0948 and a percentile interval of 0.2709-1.8932. The association remained positive, although its statistical strength depended on the uncertainty estimator.

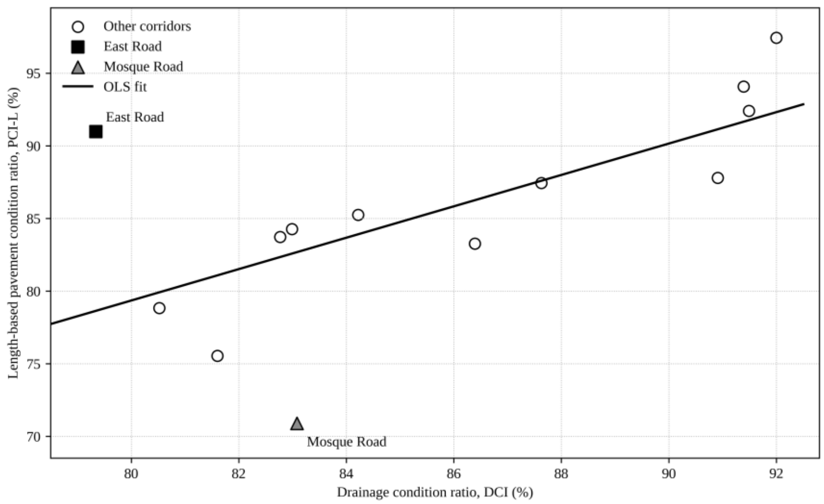

Figure 4. DCI-PCI-L association across thirteen road corridors, with East Road and Mosque Road identified.

East Road had the largest positive residual (12.34 PCI-L units) and greatest influence on the fitted slope, while Mosque Road had the largest negative residual (-11.78). Removing East Road increased the slope to 1.5023 and R^2 to 0.7157; removing Mosque Road reduced the slope to 0.9390 and produced R^2 = 0.4809. The slope remained positive in both deletions. Across leave-one-out predictions, MAE was 4.64, RMSE 6.64 and MAPE 5.56 per cent.

Table 4. Influence and leave-one-out sensitivity results for the DCI-PCI-L model

Statistic	Full model	Without East Road	Without Mosque Road
Slope	1.0801	1.5023	0.9390
Slope SE	0.3757	0.2994	0.3085
Slope p-value	0.0151	0.0005	0.0124
Slope 95% CI	0.2531 to 1.9071	0.8352 to 2.1695	0.2516 to 1.6263
R^2	0.4290	0.7157	0.4809
Adjusted R^2	0.3771	0.6873	0.4290
Held-out prediction	Not applicable	74.69	84.06
Held-out error	Not applicable	+16.29	-13.16

Note: Held-out error = observed PCI-L - predicted PCI-L.

4. Discussion

4.1 Land-cover transformation and hydrological interpretation

The sustained shift towards built-up surfaces reduced the mapped share of vegetation and bare land that supports interception, temporary storage and infiltration. The pattern is consistent with urban-hydrology research linking loss of permeable surfaces with increased runoff and flood risk (Fletcher et al., 2013; Idowu & Zhou, 2021; Zhang et al., 2022). Dynamic World has regional and class-level accuracy variation, so the Aba areas are comparative benchmark estimates rather than error-free measurements (Venter et al., 2022). The partial-year 2015 coverage also supports cautious temporal interpretation.

The findings do not imply that impervious expansion alone explains urban flooding. Spatial planning, drainage infrastructure, environmental management, governance and maintenance also shape flood occurrence and severity (Abeka et al., 2020; Fayomi et al., 2024; Wagner et al., 2021). The increase in Cw therefore indicates relative land-cover-related runoff propensity, not design runoff. Hydrological estimation requires event rainfall, infiltration, terrain, connected impervious surfaces, sub-catchments, inlet and conveyance characteristics, outlets and receiving-system performance. Similar modelling work emphasises local infiltration and calibrated hydrological inputs (Bashar and Uddin, 2025; FHWA, 2024).

4.2 Drainage-pavement association and robustness

The positive DCI-PCI-L relationship agrees with established pavement behaviour: blocked or damaged drainage prolongs ponding and promotes moisture infiltration, reducing layer and subgrade strength under traffic (Chu et al., 2023; Mousavi et al., 2021; Silva et al., 2021). The fitted model explains 42.90 per cent of PCI-L variation, so drainage is meaningful but only one part of a multivariable pavement process involving traffic, age, structure, materials, construction, subgrade, flood exposure and maintenance. This interpretation is consistent with pavement asset analytics and evidence that drainage-pavement relationships vary with local conditions and assessment methods (Piryonesi and El-Diraby, 2020).

Robustness diagnostics qualify the conventional p-value. OLS gave $p = 0.0151$, HC3 gave $p = 0.0553$ and the bootstrap interval remained positive. East Road and Mosque Road also showed corridor-specific variation beyond DCI, directing attention to structure, traffic, materials, and subgrade and maintenance history. PCI-L is appropriate for network-level screening here, while project-level rehabilitation decisions require the full ASTM D6433 procedure together with structural and material evaluation.

4.3 Scale-aware interpretation

The scale-aware framework avoids pooling city-scale land-cover observations with road-corridor measurements. City-scale results identify broader hydrological pressure and locations requiring detailed hydrological assessment, while corridor results identify roads requiring closer drainage and pavement investigation. This separation supports planning and maintenance decisions without presenting the screening indicators as calibrated hydraulic or causal pavement models.

5. Engineering implications and recommendations

Planning and drainage agencies should maintain a verified analytical boundary and complete records of GIS inputs, coordinate reference systems and processing procedures. A georeferenced study-area map should identify the thirteen surveyed road corridors and their route limits within the Aba analytical boundary and be linked to drainage and pavement-condition records for maintenance prioritisation and repeat field assessment.

East Road, Okigwe Road, Ezi-Ukwu Road and Mosque Road require detailed investigation under the study's screening rule. Assessment should address drainage continuity, blockage, sediment, geometry, outlets and hydraulic performance together with pavement structure, materials, subgrade condition, traffic, flood exposure and maintenance history. Design-level drainage upgrading should use event rainfall, current intensity-duration-frequency relationships, hydrologic soil groups, connected impervious area, sub-catchment delineation, drain dimensions, slope, roughness, inlet efficiency, conveyance capacity, outlet performance and observed discharge or flood records (FHWA, 2024). Short-duration rainfall, drainage-system variability and uncertainty should also be incorporated in design assessment (Wang et al., 2024).

6. Conclusion

Between 2015 and 2025, built-up area increased by 157.55 km², vegetation declined by 151.03 km² and Cw increased from 0.710650 to 0.854725, indicating greater relative runoff propensity under the 2025 land-cover configuration. Across thirteen road corridors, DCI and PCI-L were positively associated, with the fitted model explaining 42.90 per cent of observed PCI-L variation. OLS gave $p = 0.0151$, HC3 gave $p = 0.0553$ and the bootstrap interval remained positive. East Road, Okigwe Road, Ezi-Ukwu Road and Mosque Road were high-priority corridors under the study criterion.

The results support land-cover-informed planning, drainage inspection and targeted pavement assessment rather than a causal or design-level pavement model. Predictive and engineering-design applications require verified geospatial boundaries, event-based hydrological and hydraulic data, traffic loading, pavement structure, material properties, subgrade conditions and comprehensive maintenance records.

References

Abeka, E., Asante, F. A., Laube, W., & Codjoe, S. N. A. (2020). Contested causes of flooding in poor urban areas in Accra, Ghana: An actor-oriented perspective. Environment, Development and Sustainability, 22, 3033–3049. https://doi.org/10.1007/s10668-019-00333-4.

Bashar, T., & Uddin, M. Z. (2025). Effects of land use change on surface runoff and infiltration: The case of Dhaka City. Urban Science, 9(12), 497. https://doi.org/10.3390/urbansci9120497.

Brown, C. F., Brumby, S. P., Guzder-Williams, B., Birch, T., Brooks Hyde, S., Mazzariello, J., Czerwinski, W., Pasquarella, V. J., Haertel, R., Ilyushchenko, S., Schwehr, K., Weisse, M., Stolle, F., Hanson, C., Guinan, O., Moore, R., & Tait, A. M. (2022). Dynamic World, near real-time global 10 m land use land cover mapping. Scientific Data, 9, 251. https://doi.org/10.1038/s41597-022-01307-4.

Chu, X., Campos-Guereta, I., Dawson, A., & Thom, N. (2023). Sustainable pavement drainage systems: Subgrade moisture, subsurface drainage methods and drainage effectiveness. Construction and Building Materials, 364, 129950. https://doi.org/10.1016/j.conbuildmat.2022.129950.

Fayomi, G. U., Onyari, E. K., & Jaiyeola, A. T. (2024). Quantitative assessment of open drainage and storm water runoff capacity in Nigeria: Consequences and way forward. Case Studies in Chemical and Environmental Engineering, 9, 100766. https://doi.org/10.1016/j.cscee.2024.100766.

Federal Highway Administration. (2024). Urban drainage design manual (Hydraulic Engineering Circular No. 22, 4th ed., FHWA-HIF-24-006). U.S. Department of Transportation. https://www.fhwa.dot.gov/engineering/hydraulics/library_arc.cfm?id=189&pub_number=22.

Fletcher, T. D., Andrieu, H., & Hamel, P. (2013). Understanding, management and modelling of urban hydrology and its consequences for receiving waters: A state of the art. Advances in Water Resources, 51, 261–279. https://doi.org/10.1016/j.advwatres.2012.09.001.

Funk, C., Peterson, P., Landsfeld, M., Pedreros, D., Verdin, J., Shukla, S., Husak, G., Rowland, J., Harrison, L., Hoell, A., & Michaelsen, J. (2015).

The climate hazards infrared precipitation with stations: A new environmental record for monitoring extremes. Scientific Data, 2, 150066. https://doi.org/10.1038/sdata.2015.66.

Google Earth Engine. (n.d.-a). CHIRPS Daily: Climate Hazards Group InfraRed Precipitation with Station Data, Version 2.0 Final [Data catalogue]. Retrieved 18 July 2026, from https://developers.google.com/earth-engine/datasets/catalog/UCSB-CHG_CHIRPS_DAILY.

Google Earth Engine. (n.d.-b). Dynamic World V1 [Data catalogue]. Retrieved 18 July 2026, from https://developers.google.com/earth-engine/datasets/catalog/GOOGLE_DYNAMIC WORLD_V1.

Idowu, D., & Zhou, W. (2021). Land use and land cover change assessment in the context of flood hazard in Lagos State, Nigeria. Water, 13(8), 1105. https://doi.org/10.3390/w13081105.

Mousavi, S., Ghayoomi, M., & Dave, E. V. (2021). A system dynamics framework for mechanistic analysis of flexible pavement systems under moisture variations. Transportation Geotechnics, 30, 100619. https://doi.org/10.1016/j.trgeo.2021.100619.

Ogbonna, C. E., Ike, F., & Okwu-Delunzu, V. U. (2015). Spatial assessment of flood vulnerability in Aba Urban using Geographic Information System technology and rainfall information. International Journal of Geosciences, 6, 191–200. https://doi.org/10.4236/ijg.2015.63013.

Olofsson, P., Foody, G. M., Herold, M., Stehman, S. V., Woodcock, C. E., & Wulder, M. A. (2014). Good practices for estimating area and assessing accuracy of land change. Remote Sensing of Environment, 148, 42–57. https://doi.org/10.1016/j.rse.2014.02.015.

Piryonesi, S. M., & El-Diraby, T. E. (2020). Data analytics in asset management: Cost-effective prediction of the pavement condition index. Journal of Infrastructure Systems, 26(1), 04019036. https://doi.org/10.1061/(ASCE)IS.1943-555X.0000512.

Silva, M. F. da, Ribeiro, M. M. P., Furlan, A. P., & Fabbri, G. T. P. (2021). Effect of compaction water content and stress ratio on permanent deformation of a subgrade lateritic soil. Transportation Geotechnics, 26, 100443. https://doi.org/10.1016/j.trgeo.2020.100443.

Venter, Z. S., Barton, D. N., Chakraborty, T., Simensen, T., & Singh, G. (2022). Global 10 m land use land cover datasets: A comparison of Dynamic World, World Cover and Esri Land Cover. Remote Sensing, 14(16), 4101. https://doi.org/10.3390/rs14164101.

Wagner, S., Souvignet, M., Walz, Y., Balogun, K., Komi, K., Kreft, S., & Rhyner, J. (2021). When does risk become residual? A systematic review of research on flood risk management in West Africa. Regional Environmental Change, 21, 84. https://doi.org/10.1007/s10113-021-01826-7.

Willmott, C. J., & Matsuura, K. (2005). Advantages of the mean absolute error (MAE) over the root mean square error (RMSE) in assessing average model performance. Climate Research, 30, 79–82. https://doi.org/10.3354/cr030079.

Zhang, X., Liu, L., Zhao, T., Gao, Y., Chen, X., & Mi, J. (2022). GISD30: Global 30 m impervious-surface dynamic dataset from 1985 to 2020 using time-series Landsat imagery on the Google Earth Engine platform. Earth System Science Data, 14, 1831–1856. https://doi.org/10.5194/essd-14-1831-2022.